The bromine mediated electrosynthesis of ethylene oxide from ethylene in continuous flow-through operation

The bromine mediated electrosynthesis of ethylene oxide from ethylene in continuous flow-through operation

Jonathan Schalck[1, 2], Jonas Hereijgers[1], Wim Guffens[2], Tom Breugelmans[1,*]

[1] *Research group Applied Electrochemistry & Catalysis, University of Antwerp, Universiteitsplein 1, 2610 Wilrijk, Belgium.*

[2] *BASF Antwerp NV, Scheldelaan 600, Antwerp 2040, Belgium*

[*] *Corresponding author: e-mail: tom.breugelmans@uantwerp.be*

Keywords

Ethylene oxide, Bromine mediation, Design of an electrochemical flow-through reactor

Abstract

In this work a reactor setup for the bromine mediated, electrochemical oxidation of ethylene oxide from ethylene was developed. This novel design featured a flow- through configuration for the ethylene feed to accommodate the in situ synthesis of the 2-bromoethanol intermediate, creating a low pH at the anolyte to selectively target the bromine evolution. The cell was characterized via chronopotentiometry in 0.5 M KBr electrolyte, using a (i) Pt or (ii) IrO_2 coated gas diffusion anodes paired with a Ni foam cathode. Within a current density of 65 to 156 mA/cm² for Pt and 65 to 133 mA/cm² for IrO_2, the productivity and selectivity of the reactor system was mapped. Throughout all conditions the reactor system retained a Faradaic efficiency of 80 to 90% towards ethylene oxide on both Pt and IrO_2 coated gas diffusion anodes and exceeded an equivalent ethylene oxide production of 1 kg/hour/m² at 156 mA/cm². Furthermore, the reactor upheld identical selectivity and productivity for 4.5 hours without any signs of fading performance. Analysis of the gaseous product phase at this highest current condition showed no CO_2 or O_2 side products, originating from hydrocarbon overoxidation or oxygen. Based on our findings, the bromine mediated pathway proves to be highly promising as the current best case of the chlorine mediated system achieves a 70% selectivity towards ethylene oxide. Additionally, the anodic catalyst stability was quantified by ICP-MS analysis and scanning electron microscopy coupled with energy dispersive X-ray analysis, which revealed IrO_2 to be three orders of magnitude more dissolution resistant compared to Pt and confirm a homogeneous dispersion of the catalyst and binder material on the surface of the gas diffusion electrodes.

Introduction

Ethylene oxide (EO), or oxirane, is a key commodity chemical, representing an indispensable link in the C_2 valorization chain of the organochemical industry. Characterized for being the shortest cyclic ether, EO is inherently coupled to high molecular ring tension. Consequently, EO is a versatile base chemical for the industry enabling the synthesis of a wide variety of high(er) value chemicals. Approximately 65% of all EO is processed in its glycol form for polymer synthesis - e.g. PET, PUR and PEG - and antifreeze manufacturing [1][2][3][4]. The remaining 35% accounts for products derived from EO alkoxylation reactions that are mainly represented by surfactant, ethanolamine solvent and glycol ether solvent synthesis [2][4]. Due to ever increasing demand, the global, annual production has more than doubled in the past two decades from 15-16 Mton/year in 2000 to 35 Mton/year in 2018, and is estimated to grow an additional 2% per year in the near future [2][5][6]. With these production rates, EO is situated among the fifteen most produced chemicals in industry [7]. The current industrial standard for large-scale EO production proceeds through partial oxidation (P.O.) of ethylene. In this catalytically driven method oxygen (O_2) and ethylene (C_2H_4) are fed onto an Ag-Al_2O_3 fixed bed at approximately 250°C (Eq.1) [6][8][9]. Mechanistically, both O_2 and C_2H_4 adsorb onto the Ag sites in accordance to the Langmuir-Hinselwood model and recombine exothermally into EO [6]. The most predominant side reactions result in CO_2 formation triggered by the full combustion of ethylene feed as well as the EO product itself (Eq. 2 and 3). The EO selectivity is dependent on process parameters including the residence time and temperature and, even more, on adsorption behavior of O_2 [4]. Through extensive catalyst development - i.e. Ag catalyst activation, alloying and morphology optimization - and the implementation of moderator gases the EO selectivity in P.O. processes significantly improved from 50% in 1950 to 90% in current production plants [4][6][9][10]. However an EO selectivity of 80 to 85% was

already achieved in 1970, meaning that the overall effort in the last fifty years only resulted in negligible improvements [5][6][9][10] .

$$C_2H_4 + \frac{1}{2}O_2 \rightarrow C_2H_4O \qquad \left(\Delta H_r^0 = -105.07 \frac{kJ}{mol}\right) \qquad \textbf{Eq. 1}$$

$$C_2H_4 + 3\,O_2 \rightarrow 2\,CO_2 + 2\,H_2O \qquad \left(\Delta H_r^0 = -1411.2 \frac{kJ}{mol}\right) \qquad \textbf{Eq. 2}$$

$$C_2H_4O + \frac{5}{2}\,O_2 \rightarrow 2\,CO_2 + 2\,H_2O \qquad \left(\Delta H_r^0 = -1306.0 \frac{kJ}{mol}\right) \qquad \textbf{Eq. 3}$$

$$2\,H_2O \rightarrow 4\,H^+ + O_2 + 4\,e^- \qquad (1.229\ \text{V vs. SHE [11]}) \qquad \textbf{Eq. 4}$$

Given the annual production of 35 Mton EO per year at 90% EO selectivity, the direct greenhouse gas (GHG) emissions of P.O. reactors correspond to an estimated 7 Mton of CO_2 worldwide. In light of the global warming challenges, various countries hold businesses increasingly accountable for anthropogenic GHG emissions through taxations. For example the European Union progressively caps the total amount of GHG emissions year by year by means of mandatory allowance certificates to which all carbon heavy businesses in the affiliated countries need to comply [12]. As a result, the taxes per metric ton CO_2 equivalent become increasingly expensive and will challenge the economic viability of carbon heavy processes such as the P.O. process in the near future. Therefore, the development of ecological synthesis routes is paramount.

As such, the electro-oxidation of ethylene to EO offers a viable, CO_2 free, ecological pathway. In literature both direct and indirect - i.e. halide mediated - electrosynthesis routes have been examined [13][14]. The direct electrosynthesis is reported to be heavily impeded by the mass transfer limitation of ethylene and requires a high working potential, leading to over oxidation (OOxR) of hydrocarbons towards CO_2, as displayed in section 3 of the supplementary information. According to literature, even for current densities below 100 mA/cm² the EO selectivity was marginal [13]. Consequently the EO production characteristics for this approach are far too low to be of any significance in an industrial context. In that respect, the indirect

chlorine mediated pathway on the other hand exhibits substantially higher EO production rates, with a reported best case of 300 mA/cm² current density at 70% Faradaic efficiency over a time span of 100 hours [13][15][16]. While chlorine mediated systems have shown promising results in EO production and benefit from the vast experience regarding chlorine evolution through the well-established chlor-alkali process, a bromine mediated pathway holds several fundamental advantages over the chlorine mediated one. (i) Thermodynamically the standard reduction potential of the bromine evolution reaction (BER) is situated at 1.07 V, which is considerably lower compared to 1.36V of the chlorine evolution (CER) (Figure 1). Consequently the BER thermodynamically allows for a lower overall cell voltage which leads to a superior power efficiency. (ii) Furthermore, the BER facilitates a 100% selective halogen evolution regime at moderate pH as the difference in the thermodynamical onset potential between the BER and oxygen evolution reaction (OER, Eq. 4) is larger as opposed to the CER-OER system. (iii) Unlike Cl_2, Br_2 is moderately soluble in aqueous environment (i.e. 34 g/L at room temperature) [17][18], which omits phase separation of the halogen prior to the intermediate formation (Figure 2). Consequently, unlike Cl_2, the Br_2 reactant remains readily available in the aqueous phase to promote the reaction of ethylene to 2-bromoethanol (BrEtOH). (iv) Given that all bromine derived products, including EO, and bromine itself are moderate to highly soluble in aqueous media, i.e. the electrolyte, ethylene is the only gaseous component at anode side - provided no OER or OOxR occurs at the anode. Therefore ethylene can be fed in excess in a recycle loop without requiring any downstream purification steps, suppressing the formation of the 1,2-dibromoethane (Br_2Et) side product.

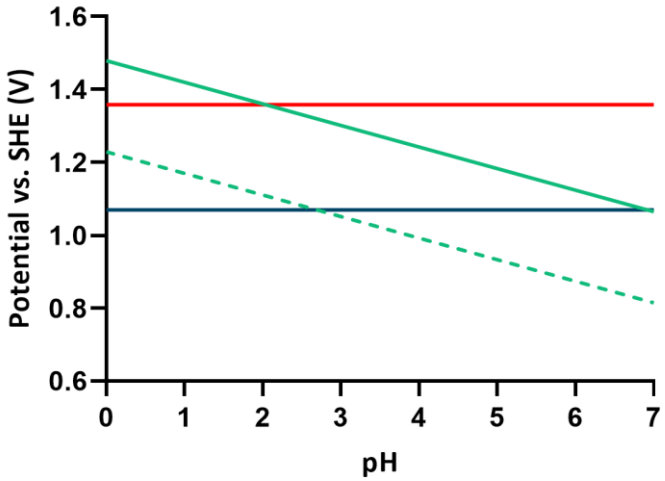

Figure 1: Pourbaix diagram of the CER chlorine evolution reaction (red), BER bromine evolution reaction (blue), OER oxygen evolution reaction (green dotted) and the inhibited oxygen evolution reaction (green) versus a standard hydrogen electrode reference [11]**.**

As mentioned the bromine mediated pathway exhibits clear advantages over the chlorine mediated pathway, yet - to the best of our knowledge - a bromide mediated epoxidation system is only studied in a handful of publications [19][20]. In both instances the BER was carried out on carbon electrodes and reactions were performed in respectively an undivided, spinning electrode setup and a trickle bed reactor. Given the shortage of research in the field of bromine mediated epoxidation and the outdated design approaches for used reactor systems, the goal of this work was to develop a highly selective, novel reactor design for the bromine mediated electrosynthesis of EO accompanied by an in depth performance study to showcasing its potential as an alternative EO production method. As such this work features, for the first time in bromine mediated epoxidation research, a divided electrochemical reactor, incorporating a flow-through configured ethylene feed to accommodate the in situ synthesis of the 2-bromoethanol intermediate. Considering the reaction mechanism, displayed in Figure 2, this design approach was critical for highly selective BER at the anode, as discussed below. In specific, this work studied the selectivity, productivity and catalyst stability of the flow-through reactor system for Pt and IrO_2 based anodes within a current density range of 65 to 156 mA/cm².

Furthermore these parameters were correlated to pH and voltage data to create a complete picture of the reactor's behavior.

The bromine mediated mechanism, presented by Figure 2, is a combination of an electrochemical and organochemical system, in which the anodic oxidation and cathodic reduction act as supply reactions for necessary reactants to carry out reaction step 2 and 4 towards EO synthesis. As such the anode carries out the BER (1.07 V vs. SHE [21]) and at the cathode side the alkaline hydrogen evolution reaction, i.e. alkaline HER (0 V vs. RHE [11]), takes place. Since bromide is released in reaction step 4 the reactions form a closed loop system, reusing the released bromides at the anode side. The conversion step of ethylene to BrEtOH (step 2) is carried out in the vicinity of the anode as well. The release of protons in this reaction step acidifies the anolyte to establish reaction conditions in favor of the BER. Meanwhile the alkaline HER proceeds completely selective, provided the alkalinity of the catholyte is sufficiently high, as these conditions omit the interference of the acidic HER. Critically only the alkaline HER provides the hydroxyl ions to (i) synthesize EO and (ii) self sustains its thermodynamically favorable pH window. Since both the anolyte and catholyte in situ become respectively acidic and alkaline, given the BrEtOH synthesis is accommodated in the anolyte compartment, a membrane divided reactor setup establishes a pH difference to comply with the optimal reaction conditions of the electrochemical half reactions. Therefore the electrolyte feeds can consist solely of neutral salt solutions. Furthermore separating the anode and cathode with a membrane prevents hydrocarbon crossover towards the cathode. In specific, this work focusses on the influence of current density on the selectivity and productivity as well as the catalyst stability in chronopotentiometric steady state operation.

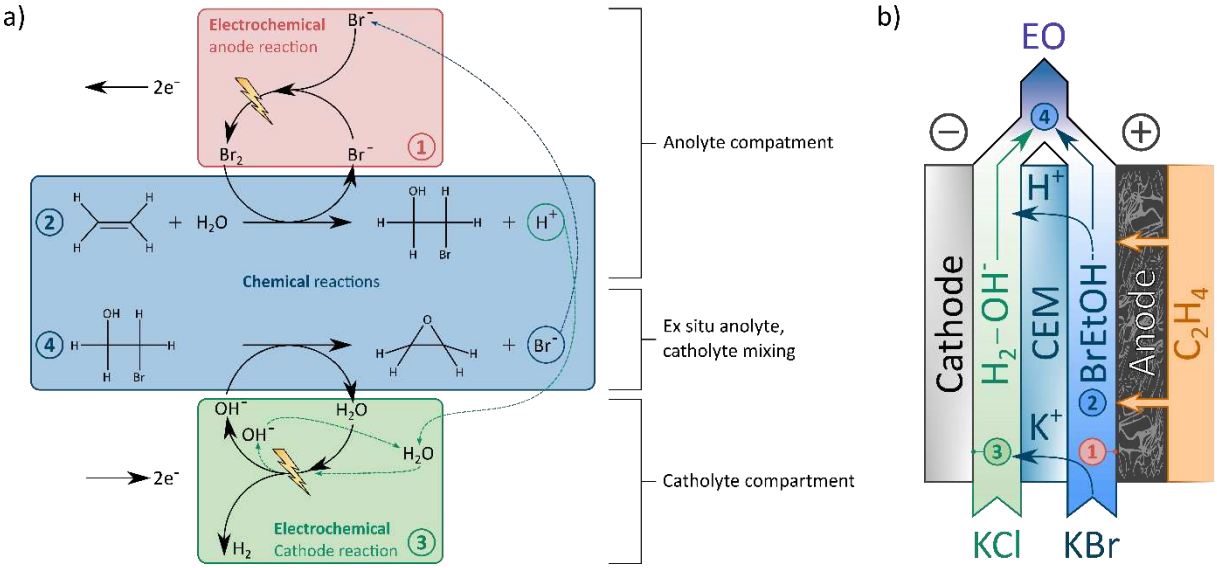

Figure 2: The indirect, halide mediated electro-oxidation of ethylene to EO. 4a) Displays the mechanism and 4b) shows the implementation of each step in the flow through reactor setup.

Materials and methods

1. Gas diffusion electrode manufacturing

Pt or IrO_2 based gas diffusion electrodes (GDE's) were implemented as porous anode in the EO reactor. To this end carbon based gas diffusion layer substrates (GDL 39 BB - Ion Power) were coated with a catalyst ink suspensions consisting of a Nafion® binder (5wt% D-521 suspension Alfa Aesar), 2-propanol (Chem-Lab), ultrapure water (Merck Millipore®) and active catalyst powder, which was either Pt or IrO_2 based. The catalyst to Nafion dry mass ratio was 2.3/1 and solid to liquid weight ratio was 1/100. For the liquid fraction, an IPA to H_2O ratio of 50-50 wt% was maintained [22]. In total, four coating variations were tested in the EO reactor: (i) Pt, (ii) Pt-C, (iii) IrO_2 and (iv) IrO_2-C. (i) For the Pt based GDE, a 100% platinum black powder was used (Sigma Aldrich – 205915, 25 m²/g). (ii) Pt-C GDE's were produced with 20 wt% platinum, embedded in active carbon powder (Alfa Aesar – 035849, 127 m²/g). (iii) The IrO_2 GDE was composed of pure, non-carbon supported, Ir/IrO_2 core shell particles (Fuel cell store – 3151663, 10 to 20 m²/g). (iv) The same Ir/IrO_2 core shell material was used in a blend with carbon powder (Cabot Norit® SX 1G, 1000 m²/g) yielding a 20 wt% IrO_2 catalyst for the IrO_2-C class GDE

structures. A full overview of the ink compositions and catalyst loading for each tested GDE is provided in the supplementary information in Tables S.1 and S.2. All coatings were applied on the mesoporous side of the GDL by means of a manual airbrush operation. During coating the GDL substrate was heated to 60°C on a heating plate to promote evaporation of the liquid fraction. The accuracy of the catalyst loading was determined via differential weighing before and after coating (Ohaus Explorer, Analytical line) and verified with ICP-MS analysis for Pt and Pt-C based GDE's. To this end the Pt catalyst layer was overnight quantitatively stripped from newly sprayed GDE's substrates in undiluted aqua regia at 60°C and followed by ICP-MS analysis of the acidic fraction. The aqua regia fraction was prepared for ICP-MS analysis by diluting the sample 100 times with ultrapure water (Merck MilliPore), acidification with 70% HNO_3 (Sigma Aldrich - 225711) and spiking with an yttrium based internal standard (Alfa Aesar - 11331429). The results between the differential weighing method and ICP-MS analysis deviated less than 5%, thus proving the accuracy of the weighing method.

2. Reactor setup

A graphical representation of the flow-through reactor unit is displayed in Figure 3 0.5M KBr and 0.5M KCl electrolyte solutions were respectively fed in a single pass operation into the anode and cathode compartment. A Nafion 117 cation exchange membrane (CEM) (Dupont, Fuel Cell Store- 591239), pretreated in H_2SO_4 and in H_2O_2, separates anolyte and catholyte compartment. Since the alkaline HER at the cathode is vulnerable to bromide poisoning, the catholyte was composed of 0.5 M KCl (>99.5%, Chem-Lab) [21][23][24]. The anolyte feed consisted of 0.5 M KBr (>99.5%, Chem-Lab). The Nafion 117 acted as an impervious barrier for the anions, effectively shielding the cathode from any bromide exposure. At anode side, the Pt or IrO_2 based GDE was sealed against a graphite plate with a set of Viton® gaskets (Eriks). In this anodic graphite plate a serpentine gas field was machined to evenly distribute ethylene at the GDE backside (PTFE reinforced side). Since the gas flow field was designed with a dead

end at the top side, the ethylene feed could only exit the reactor by flowing through the porous GDE structure into the anolyte flow compartment. Consequently, the anolyte flow compartment accommodated both the BER and the chemical conversion to BrEtOH intermediate (Figure 2). For accurate monitoring of the anode potential a reference electrode (RE) (3M Ag/AgCl Metrohm) was mounted into the anolyte compartment. At the cathode side a Viton gasket sealed the Ni foam against a graphite plate. Both the anode side and cathode side graphite plates were in direct contact with copper collector plates to which the positive and negative terminal of the potentiostat (Autolab PGSTAT302N) were connected. The anodic catalyst tests were performed within a runtime window of 7 minutes. In a steady state regime the liquid and gaseous products were analyzed in a GC unit according to paragraph 3 “GC analysis of the liquid and gas phase” in the “Material and methods” section. Each experiment was repeated four times and for each repetition a newly coated GDE was placed at the anode side to be subjected to a complete chronopotentiometry (CP) series, starting at the lowest current density - i.e. 67 mA/cm² - up to the highest - i.e. 156 mA/cm².

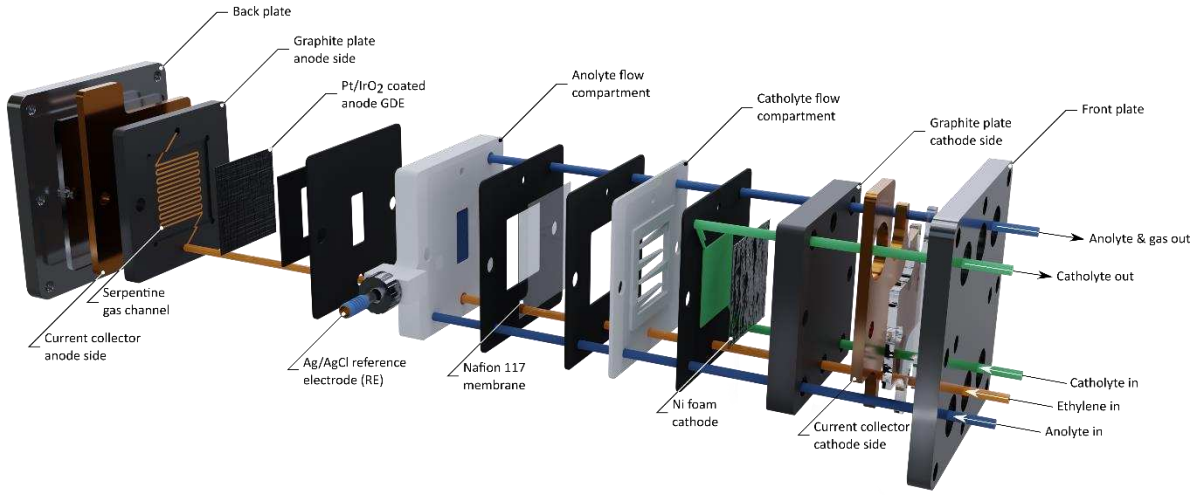

Figure 3: Exploded view of the continuous, flow-through reactor unit

A peripheral control system was constructed to enable accurate process control and to monitor the reactor during operation, as represented in Figure 4. The ethylene gas feed was controlled by a mass flow controller unit (MFC) (Aalborg, 0-200 sccm) at 15mL/min. The electrolyte feed

rates were regulated at 15 mL/ min as well with a set of pulse width modulated membrane pumps (White Knight). The anolyte product flow was divided in a gaseous and liquid phase by a gas liquid separator unit. As such samples drawn from the headspace of the gas-liquid separator were analyzed for possible OER and OOxR side products in a gas chromatograph (GC). The liquid flow of the anolyte and catholyte product flow were mixed to accommodate the final conversion step of the BrEtOH intermediate into EO. Liquid samples were drawn from this combined product flow for GC analysis. Since the pH is a critical parameter in terms of reactor selectivity and overall performance, an in-line system was constructed (Metrohm) capable of monitoring and logging the pH of both the anolyte and catholyte product flows to allow for an in depth selectivity versus pH correlation study. Additionally a temperature sensor was installed to improve the accuracy of the pH measurement.

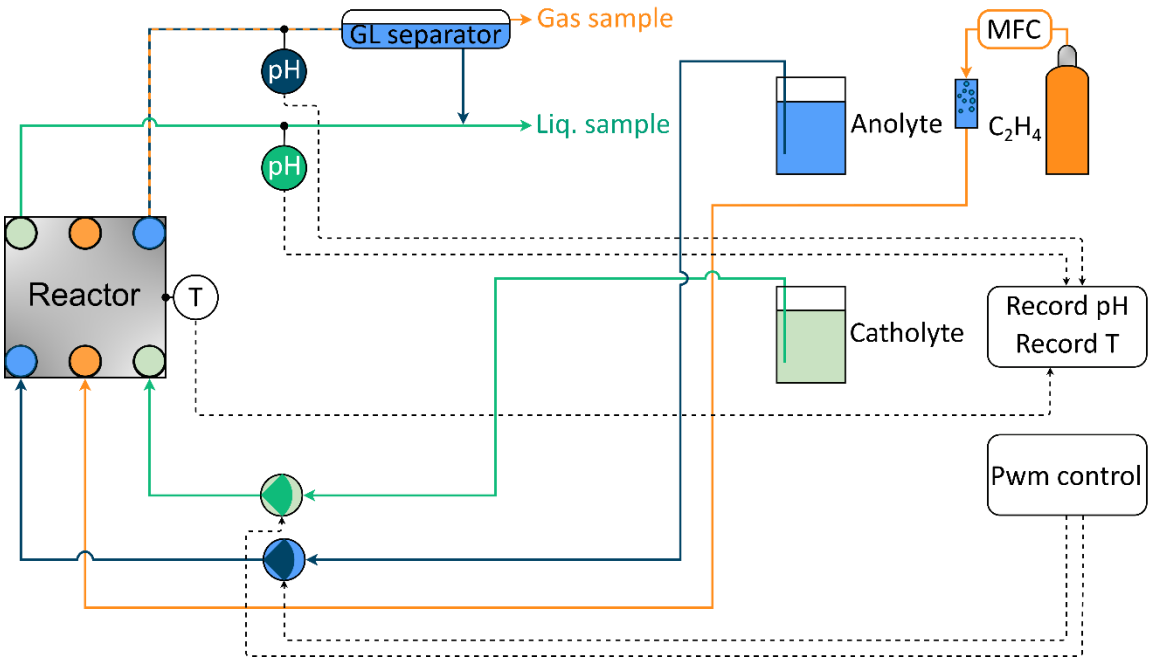

Figure 4: P&ID schematic of the setup, displaying the peripheral control and data acquisition systems.

3. GC analysis of the liquid and gas phases

All liquid phase products were off-line quantified on a GC-FID system (Interscience Focus) fitted with a polar column (Restek Stabilwax). The GC unit was calibrated for a variety of

components such as methanol, ethanol, isopropanol, 2-propanol, methoxyethane, 2-bromoethanol, 1,2-dibromoethane, ethylene oxide and mono-, di-, tri- and polyglycol. For the off-line analysis the anolyte and catholyte product flow were sampled for 2 minutes. From this liquid reactor sample, 1 mL was transferred to a GC vial to which 3 µL of 1-propanol was added as internal standard. The sample injection was carried out by an autosample unit (Thermo Scientific AI 1310) equipped with a 0.5 µL syringe. The injection volume was set at 0.3 µL and the inlet and detector temperature set points were respectively 250°C and 300°C.

The gas phase samples of the anolyte were manually injected in a GC-TCD system (Shimadzu GC 2014 - Restek Shincarbon ST) and checked for the presence of O_2 and CO_2, respectively originating form unwanted OER and OOxR at the anode. The gas samples were drawn from the headspace of the liquid-gas separator with a syringe, fitted with a valve system to seal the compartment air tight. A more detailed description of the gas phase analysis method is provided in the supplementary information document in section 2 “Gas analysis”.

4. Selectivity and productivity calculations

Throughout this work the Faradaic efficiency (FE) is used as a measure for the reactor’s selectivity. The equations to calculate the FE from the GC analysis data and flow rates are provided in the supplementary information (Eq. S.2 and Eq. S.3). To minimize the accuracy error on the liquid flow rate, the flow rate is derived from sampling time, sample weight and the mass density data as opposed to relying on the pump set point value. The latter parameter, i.e. the mass density of the liquid product flow, was determined by weighing a pipetted volume of 5 mL for each drawn sample.

5. Stability: ICP-MS measurements and calculations

The catalyst dissolution and detachment degradation was investigated via ICP-MS (Aligent 7500 Series). To this end the dissolution and total catalyst loss were respectively quantified by (i) the catalyst content in the anolyte for each tested current density and (ii) the catalyst loading

on the GDE before and after a complete CP series, i.e. after five current density runs (65 to 156 mA/cm²). (i) For dissolution the samples were prepared for ICP-MS analysis according to the dilution, acidification and spiking protocol described in paragraph 1. (ii) For the total catalyst loss, coatings were dissolved in aqua regia as described in the paragraph 1 (following Eq. S.4). The detachment was subsequently calculated from the subtraction of the total catalyst loss and dissolution, according to Eq. S.8. This stability study coupled with the GC analysis of the product flow provided all data to deduce the stability number S, as defined by S. Geiger *et al.* (Eq. S.6) [25]. A detailed description of all used calculations is provided in the supplementary information.

6. Microscopy

SEM and EDX images are taken on a FEI Quanta 250 at 20kV. Multiple locations of the coated area of the GDE's before and after reaction were studied for a back to back comparison regarding catalyst morphology degradation due to agglomeration, reshaping or Ostwald ripening. Furthermore EDX mapping of C, K, F, O, Pt and Ir was performed to visualize the distribution of the catalyst and Nafion binder.

Results and discussion

1. Selectivity, conversion and productivity

Figure 5 depicts the selectivity, cell voltage, uncompensated and compensated anode potential for Pt, Pt-C, IrO_2 and IrO_2-C based anodes. The reactor consistently achieved a FE between 80% to 90% towards EO throughout the tested current density range, with the exception of the IrO_2-C based anode series. Furthermore a long term single pass experiment, reported in the supplementary information (section 7), achieved and sustained a FE towards EO of 84 to 93% for 4.5 hours. Compared to the best reported case of the chlorine mediated system, i.e. 70% FE towards EO, the bromine mediated mechanism in the flow-through reactor setup system

achieves a considerably higher selectivity for both the Pt and IrO_2 catalyst materials [13]. Although setup and condition differences exist (i.e. gas flowrate, no flow-through configuration, membrane type, current density, runtime, halide mediator and halide concentration) this comparison indicates that the bromine mediation mechanism in a flow-through reactor configuration proves to be a promising system, given the significantly higher FE at lower electrolyte concentration (i.e. 0.5M versus 2M). Additionally other sources on the bromine mediated reaction system, A. Manji *et al.* reports a FE towards propylene oxide of 52 to 58% between 100 to 160 mA/cm² current density, which is significantly lower than the obtained selectivity figures in this work [20].

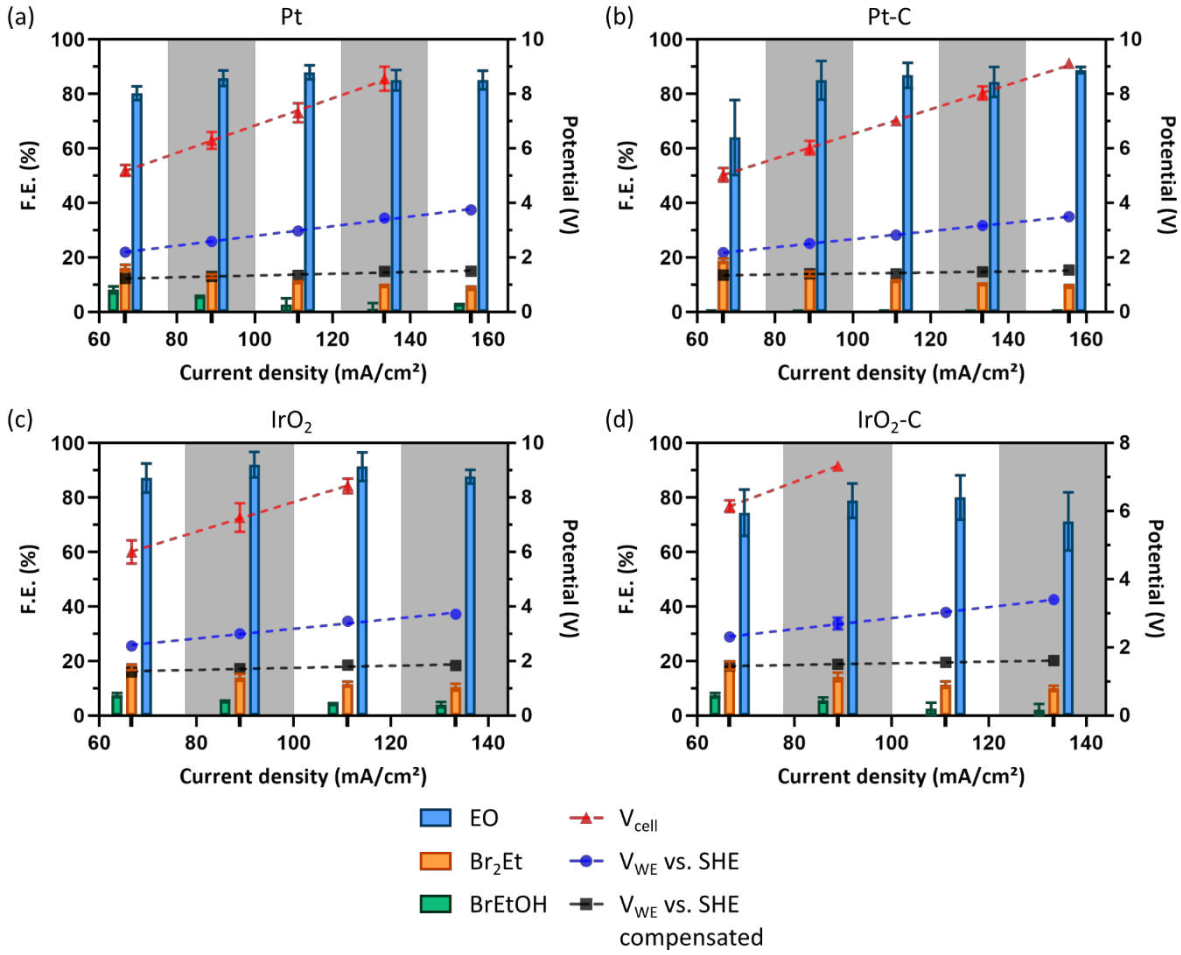

Figure 5: Results of the chronopotentiometric measurements in continuous flow-through operation at room temperature and 15 mL/min ethylene, 15 mL/min 0.5M KBr anolyte and 15 mL/min 0.5M KCl catholyte flow. The

bar graphs represent the Faradaic efficiency, on the left y-axis, of each component for (a) Pt, (b) Pt-C, (c) IrO_2 and (d) IrO_2-C based anodes. Superimposed on the bar graph the voltage related data is plotted in respect to the right y-axis.

The liquid phase of the mixed product flow (i.e. anolyte and catholyte) solely contained EO, BrEtOH and Br_2Et products, as displayed in Figure 5. Additional GC analysis on exclusively the catholyte flow was carried out to check for possible BrEtOH and Br_2Et crossover through the membrane. No bromine derived products were detected in the liquid catholyte, thus indicating that Nafion® 117 is impervious to BrEtOH and Br_2Et crossover within the achieved concentration levels in the reactor system.

The trace amounts of BrEtOH in the mixed product flow represent unreacted intermediate product that did not convert yet into EO. A higher abundance of hydroxyl ions would convert the remaining BrEtOH into EO as well. So in essence there is additional EO selectivity still to be gained, further stressing the value of the bromine mediated system over the chlorine mediated approach. The Br_2Et molecule is the product of the competing side reaction to the BrEtOH synthesis (step 2 Figure 2). Mechanistically both Br_2Et and BrEtOH are formed via a short-lived, positively charged cyclic halonium ion transition state [26][27]. (i) For BrEtOH synthesis the accepted mechanism in literature suggests a disproportionation of halogen and water according to Eq. 5. Subsequently, hypohalous acid acts as the reactive species in donating the halide, forming the cyclic halonium ion, followed by the nucleophilic addition of its hydroxyl group [13][16][19]. The bromine halogen is mildly soluble in aqueous medium, i.e. approximately 34 g/L at room temperature, which contributes to the disproportionation towards hypobromous acid and subsequent formation of BrEtOH [17][18]. (ii) The cyclic halonium state is susceptible to the nucleophilic addition of bromides as well, which yields Br_2Et. (iii) Additionally BrEtOH can decay into Br_2Et in the acidic environment of the anolyte through protonation of the alcohol group followed by a nucleophilic substitution with bromide. To minimize the effect of the acidic decay, the conversion towards EO and pH neutralization was

carried out without any delay at the reactor exhaust through extensive mixing of the anolyte and catholyte. Crucially, the formation of Br_2Et impedes the desired reaction mechanism resulting in (i) a reduction in EO productivity and (ii) the elimination of two bromide species from the anodic recycle loop as the C-X bond is no longer cleaved (step 4). In this regard, aside from the mechanistic competition between BrEtOH and Br_2Et, the ethylene feed rate and its homogeneous dispersion promotes the reaction selectivity towards BrEtOH for the instance of a high ethylene to bromine ratio [28]. With the implementation of a serpentine gas channel, a flow-through configuration and accurate ethylene feed rate control, these Br_2Et suppressing conditions could be established in practice. In specific, an excess of 15 mL/min of ethylene gas was fed through the serpentine channel into the anolyte compartment to favor the formation of BrEtOH. Figure 6 displays for each tested catalyst material and current density the conversion ratio of the excess fed ethylene oxide. At 155.5 mA/cm², the reactor converted approximately 17% of the ethylene feed utilizing Pt and Pt-C based anodes. For the IrO_2 based anodes outperform the IrO_2-C variants almost 15% conversion at 133.3 mA/cm².

$$X_2 + H_2O \rightleftharpoons XOH + XH \qquad \textbf{Eq. 5}$$

The reactor selectivity performance for each liquid product and tested current density was objectively evaluated by means of a statistical 2-way Anova test (Tukey Multiple Comparison) with a 95% confidence interval and show two conclusions. (i) The test indicated that the reactor exhibited a reduced FE of EO when utilizing an IrO_2-C based anode in comparison with the other anode variants. Furthermore the test confirmed the reactor maintained a stable selectivity towards EO throughout all tested current densities.

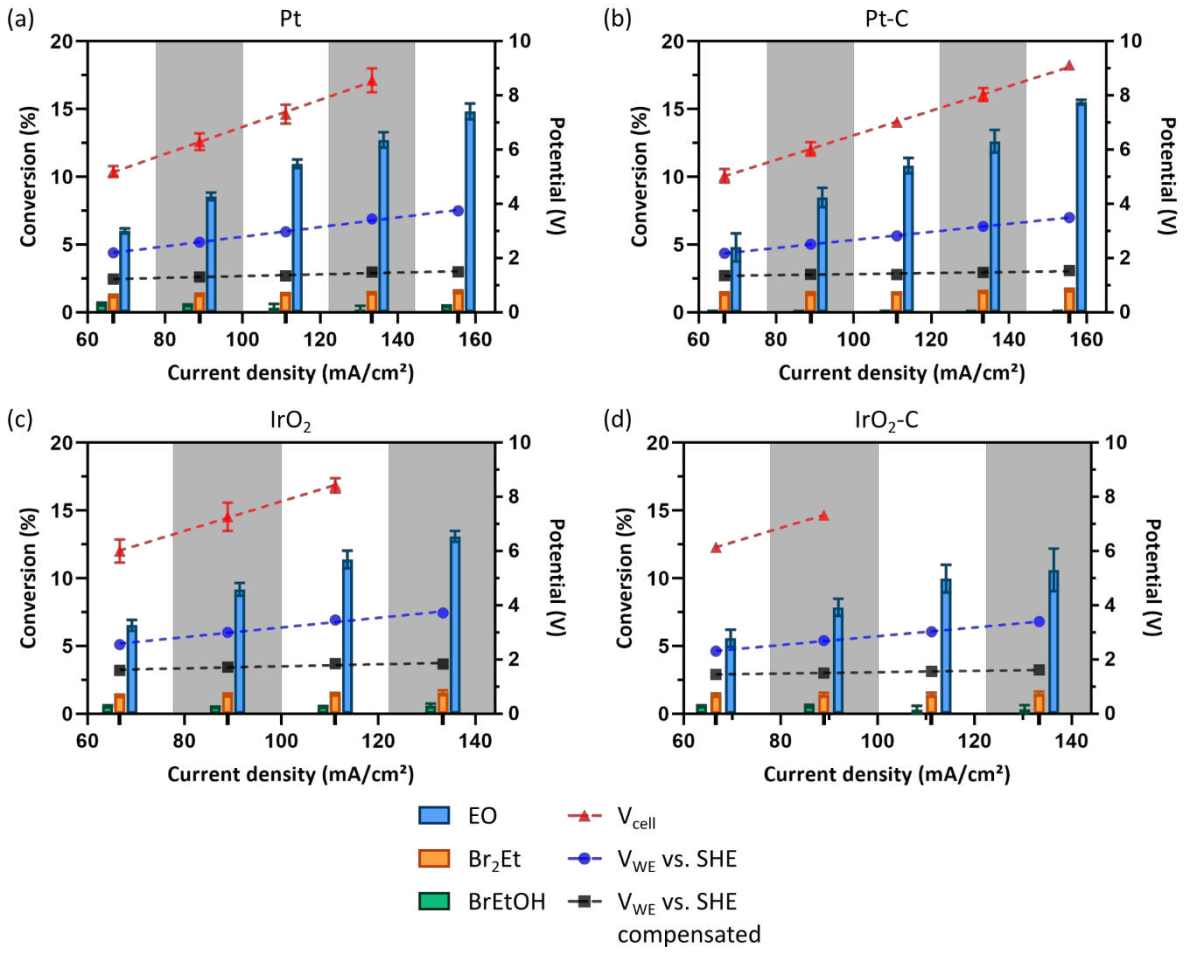

Figure 6: The conversion ratio of the ethylene feed towards BrEtOH, Br_2Et and EO in respect to the tested current density at room temperature and 15 mL/min ethylene, 15 mL/min 0.5M KBr anolyte and 15 mL/min 0.5M KCl catholyte flow for Pt, Pt-C, IrO_2 and IrO_2-C based anodes.

(ii) Secondly, for every anode material the Br_2Et selectivity showed a strong correlation with the current density, as displayed by Figure 7. Regardless of the anode material, the reactor selectivity for Br_2Et consistently decreased towards increasing current density. The disproportionation behavior of Br_2 in Eq. 5 likely causes this decreasing tendency. At high current density the BER produces more Br_2 shifting the equilibrium more towards the disproportionated HOBr form. Consequently ethylene reacting with HOBr, instead of Br_2, yields BrEtOH out of the cyclic halonium transition state, resulting in a decreased Br_2Et selectivity. As such the BrEtOH production at the anode increases. Simultaneously, at the cathode side the increased current density elevates the alkalinity of the catholyte. Due to the

increased abundance of both hydroxyl and BrEtOH, the conversion of the intermediate towards EO (step 4) more readily occurs, therefore increasing the productivity of EO and reducing the trace amounts of unreacted BrEtOH.

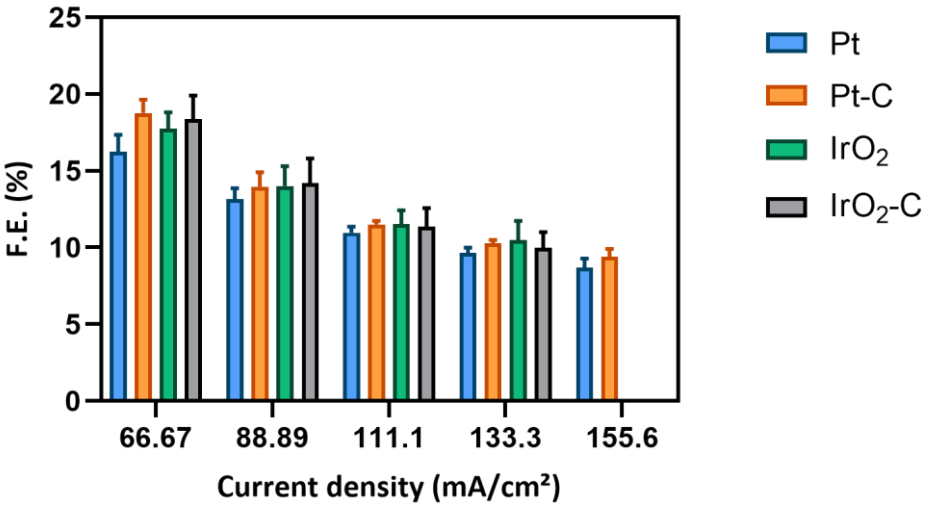

Figure 7: The correlation of the Br_2Et selectivity in respect to the tested current density at room temperature and 15 mL/min ethylene, 15 mL/min 0.5M KBr anolyte and 15 mL/min 0.5M KCl catholyte flow for Pt, Pt-C, IrO_2 and IrO_2-C based anodes.

The gas flow exiting the reactor was analyzed in order to quantify the O_2 and CO_2 content via GC to check for unwanted OER or OOxR at the anode. This analysis was carried out at 133.3 mA/cm² for IrO_2 based and 155.6 mA/cm² for Pt based catalysts, i.e. the highest tested current density for each material, as at conditions the OER and OOxR were most likely to occur. The results of the gas phase analysis are depicted on Figure S.1 in the supplementary information. In all cases the reactor did not exhibit any interference of OER or OOxR and as such the anode operated fully selective towards the BER. This is also confirmed by the fact that the cumulative FE of all liquid products equaled 100%, suggesting total charge was already fully accounted for in the liquid phase. This can be explained by the presence of halides, chloride or bromide, into the electrolyte causing an inhibition effect on the OER side reaction for concentrations as low as 10-15 mM, which originate from their strong adsorption affinity for metal surfaces

[11][21][29][23][30]. The halides tend to cover all active sites on the catalyst, effectively blocking the accessibility for oxide species, which results in an upwards shift of the OER thermodynamic onset potential [24][31][32]. For metal oxides a similar behavior was observed in rotating ring disk (RRDE) experiments by J.G. Vos *et al.* Therefore the OER onset potential for an IrO_2 catalyst in the presence of 40 mM Cl^- was in their work relocated in accordance to the solid green line in Figure 1 [11]. In general the halide inhibition facilitates selective BER and CER, but the effect is most notable for the BER due to its additional advantage of a lower onset potential.

At the 66.7 mA/cm² the anolyte and catholyte pH were respectively around 2.5 and above 11.5, starting from an pH difference of 9 units across the Nafion 117 membrane. At respectively 133 and 156 mA/cm² for IrO_2 and Pt the pH difference over the Nafion 117 membrane increases further to approximately 10 units, as the formation of BrEtOH and alkaline HER was boosted with increasing current density (Figure 8). Despite the enlarging pH gradient, a direct influence on the reactor selectivity was never observed. The reason being, the acidic and alkaline conditions at the lowest current density already met the conditions for fully selective anodic and cathodic reactions, hence the bromine derived liquid products account for 100% of the charge at all tested current densities. The reactor exhibited near identical pH values for the anolyte and catholyte product flows, regardless of the used anode catalyst. As such, all anode catalysts operated in similar conditions.

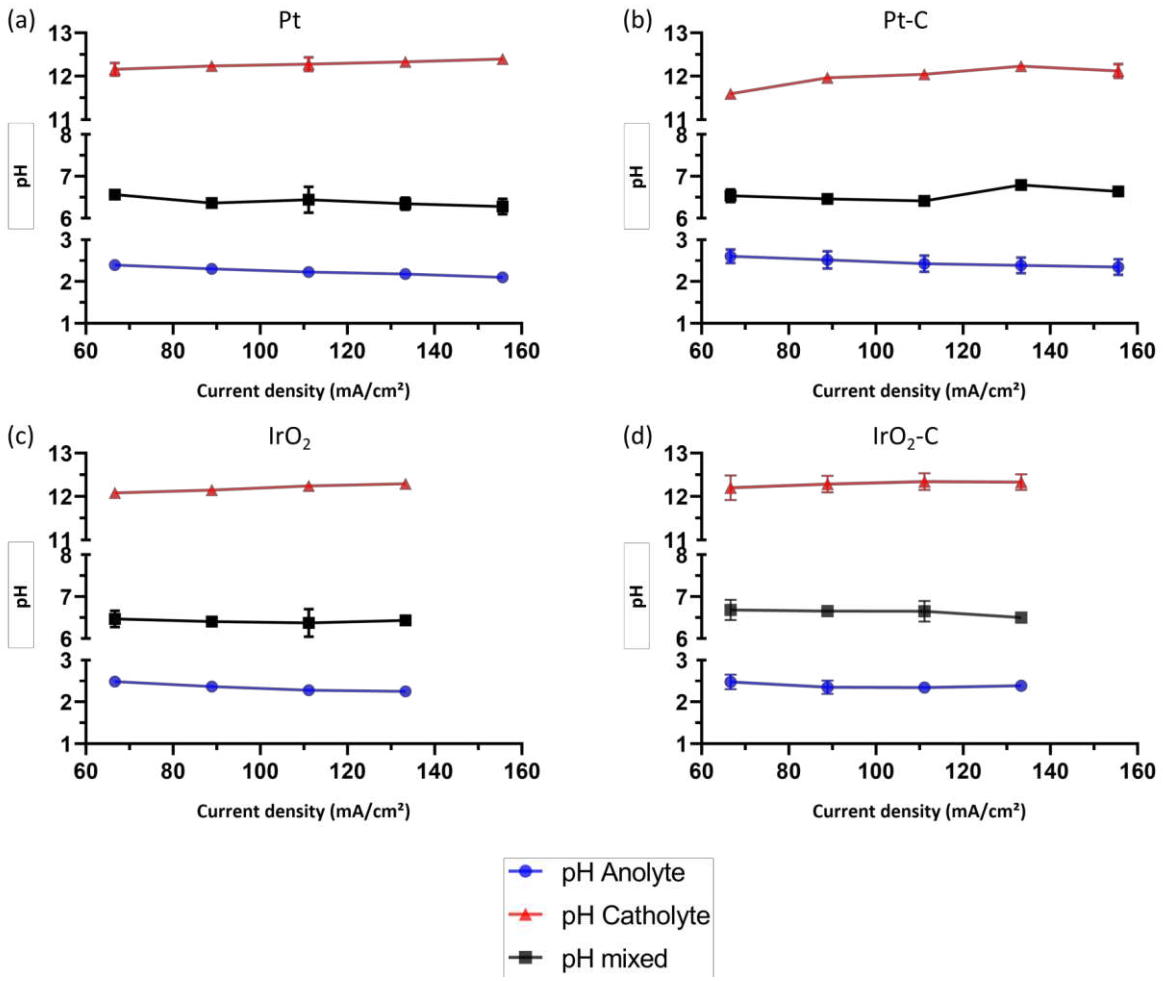

Figure 8: pH of the anolyte (blue), catholyte (red) and mixed product flow (black) at room temperature and 15 mL/min ethylene, 15 mL/min 0.5M KBr anolyte and 15 mL/min 0.5M KCl catholyte flow for (a) Pt, (b) Pt-C, (c) IrO_2 and (d) IrO_2-C based anodes.

Figure 9 displays the normalized production rate per hour and per square meter of electrode surface for each component in the liquid phase. As previously stated, the reactor exhibits a high and stable FE towards EO throughout the tested current density range - with the exception of the IrO_2-C series. Since EO is the predominant product, the reactor production exhibits a quasi linear correlation with the current density for the majority of the anodes. At the highest tested current density, i.e. 133 mA/cm² for IrO_2 and 156 mA/cm² for Pt, the reactor generated an equivalent EO output of 0.98 kg EO/hour/m² with Pt, 1.02 kg EO/hour/m² with Pt-C, 0.87 kg EO/hour/m² with IrO_2 and 0.70 kg EO/hour/m² with an IrO_2-C based anode. As a point of reference, the best reported case of the CER mediated system in highly concentrated electrolyte,

i.e. 2M KCl, achieves a production rate of 1.74 kg EO/hour/m² at a current density twice as high as the tested upper limit of the Pt based anodes in this work. Since the IrO_2-C series clearly displayed a reduced EO selectivity in Figure 5, the reactor system exhibits a significantly lower EO production for this anode material. In general these production values showcase the capability of the bromine mediated reactor system in terms of EO production. Theretofore, given the stable EO selectivity throughout the tested current density window, the production is scalable with the current density without a loss in energy efficiency.

The overlaid voltage data in Figure 5, Figure ***6*** and Figure ***9*** and displays the (i) uncompensated and (ii) compensated anode potential versus a standard hydrogen reference electrode (SHE) as well as the (iii) overall cell voltage. For each reactor assembly, the anolyte resistance and total cell resistance were measured via impedance. The anolyte resistance was consistently quantified between 5.8 to 6.3 Ohm and the total cell resistance was approximately 19 Ohm. Given this cell resistance, the cell voltage of the single pass experiments as a function of the current density. By increasing the electrolyte concentration above 0.5 M and by design optimization of the cell the internal cell resistance could be reduced, thus improving the power efficiency of the reactor system. Given the hydrogen bubble formation in the catholyte substantially affected the cell resistance, a redesign of the catholyte compartment to induce an efficient bubble evacuation would greatly improve the power efficiency of the system as well. However these optimization strategies fall outside the scope of this paper and will be investigated in future research.

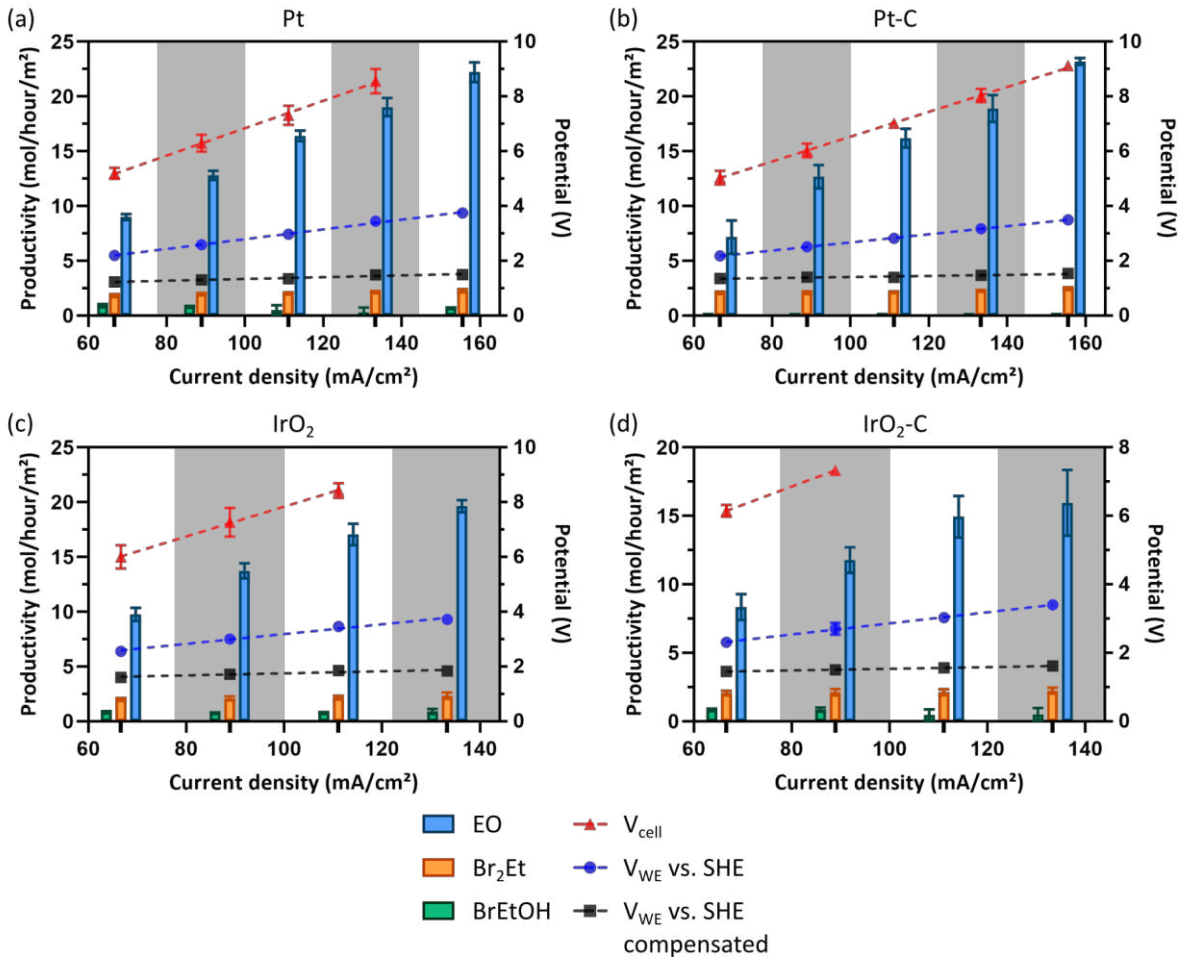

Figure 9: Results of the chronopotentiometric measurements in continuous flow-through operation at room temperature and 15 mL/min ethylene, 15 mL/min 0.5M KBr anolyte and 15 mL/min 0.5M KCl catholyte flow. The bar graphs represent the productivity per hour per m² electrode surface, on the left y-axis, towards each component for (a) Pt, (b) Pt-C, (c) IrO_2 and (d) IrO_2-C based anodes. Superimposed on the bar graph the voltage related data is plotted in respect to the right y-axis.

2. Stability analysis

The anodic catalyst stability is investigated via (i) ICP-MS analysis, to quantify for the dissolution and detachment degradation, and (ii) SEM-EDX image processing, to visualize the morphology changes in the catalyst layer after reaction - i.e. Ostwald ripening, agglomeration, pulverization and reshaping. (i) The dissolution data is provided in Figure 10. On the y-axis of this graph the stability number (S) - i.e. the ratio of the EO production per mol of dissolved catalyst, is represented as function of the current density [25]. A high S number represent a high stability as these catalysts inherently exhibit a low dissolution value. On Figure 10 IrO_2 and

IrO_2-C based GDE's show a superior stability over the Pt and Pt-C coated anodes, with IrO_2 reaching a stability three orders of magnitude higher compared to the Pt-C series, which is even an underestimation as in the majority of the electrolyte samples no IrO_2 was detected compared to the blank check. These cases represent an infinite stability number and were therefore excluded from the graph. For this reason no finite datapoints could be retrieved for the two highest current density points of the IrO_2 series. IrO_2 is commonly used as active catalyst material for the manufacturing of dimensionally stable anodes (DSA) [33]. As iridium already reached its highest oxidation state in this conductive metal oxide form, the material exhibits a high resistance towards the dissolution degradation mechanism, which matches the general trend in the data of Figure 10 [33].

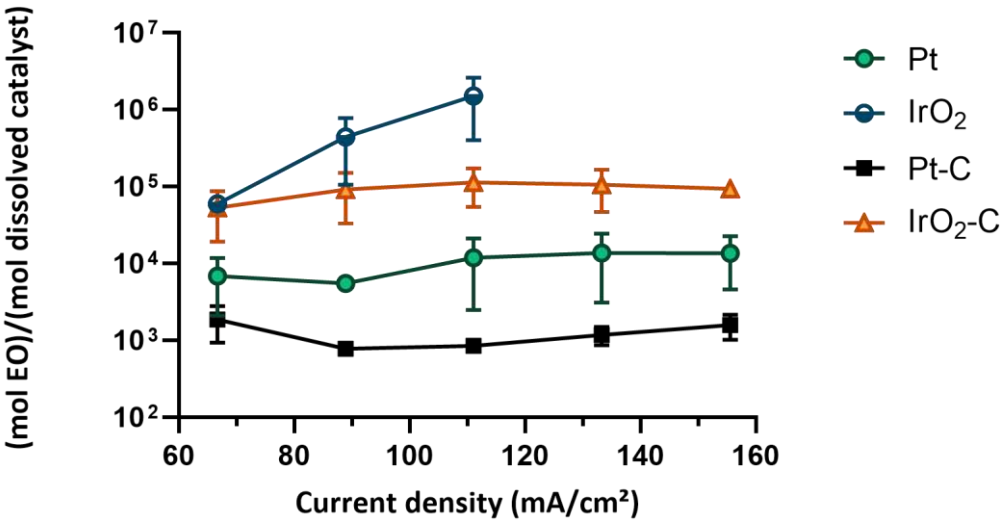

Figure 10: Disssolution degradation data at room temperature and 15 mL/min ethylene, 15 mL/min 0.5M KBr anolyte and 15 mL/min 0.5M KCl catholyte flow for Pt, Pt-C, IrO_2 and IrO_2-C based anodes. The data was retrieved via ICP-MS analysis of the anolyte according to paragraph "Stability: ICP-MS measurements and calculations" in the "materials and methods" section.

(ii) The EDX analysis for Pt, Ir, O, C, F and K was performed on all anode catalysts before (BR) and after reaction (AR) of a full CP series. Measurements showed a homogeneous distribution of the catalyst suspension, i.e. the Nafion ® binder and the (carbon supported) catalyst material, on freshly sprayed GDE's (BR). In Figure 11 fluor, and carbon for non-carbon

supported catalysts, corresponds to the location of the Nafion binder. Naturally for carbon supported catalysts, most of the carbon signal is correlated to the distribution of the catalyst itself. Potassium was only visible on the AR series as an artefact of the potassium bromide anolyte after washing. The Pt and, more apparent, the Pt-C GDE's display a reduced intensity signal for Pt AR compared to Pt BR. The Ir signal of IrO_2 and IrO_2-C anodes maintained its intensity before and after reaction. As such the EDX analysis complements the ICP-MS dissolution results of Figure 10.

Additionally Figure 11 displays the SEM analysis of all tested anode materials. The full SEM series is provided in the supplementary information. Most notably the SEM images show a crater like structures in the coating of the Pt-C GDE's, which are likely the result of the mechanical force exerted by the ethylene feed as it flows through the porous anode. As such, flow-through configuration of the reactor increases the likelihood of catalyst detachment at the anode side. With the other catalyst materials this extensive detachment was not present, but at the highest magnification slight pulverization degradation of the IrO_2 particles was revealed. Any other form of morphology degradation was not observed.

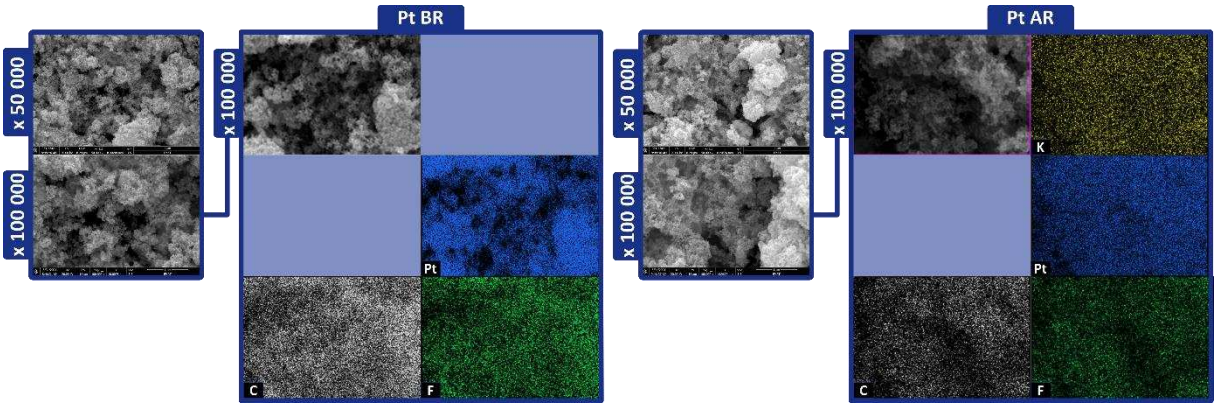

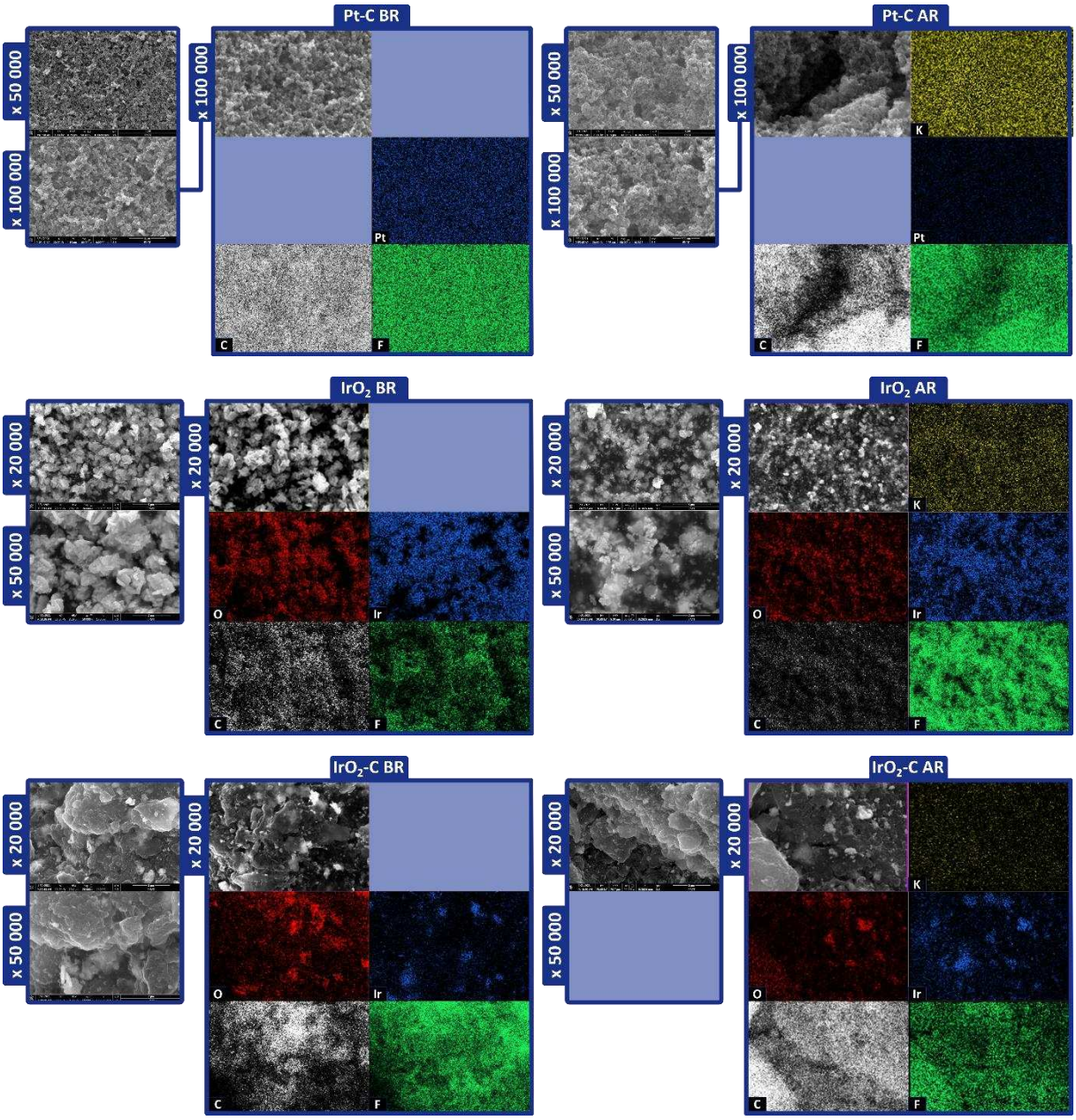

Figure 11: SEM-EDX analysis of catalyst coatings before reaction (BR) and after reaction (AR) of Pt, Pt-C, IrO_2 and IrO_2 based anodes. The AR Pt based samples underwent chronopotentiometric runs of 10 min each at 66.67, 88.89, 111.1, 133.3 and 155.6 mA/cm². The AR IrO_2 based samples underwent chronopotentiometric runs of 10 min each at 66.67, 88.89, 111.1 and 133.3 mA/cm². Tests were conducted at room temperature and 15 mL/min ethylene, 15 mL/min 0.5M KBr anolyte and 15 mL/min 0.5M KCl catholyte flow. The electron microscopy images were obtained on a FEI Quanta 250 at 20kV.

Since the SEM analysis visualized possible detachment degradation in the Pt-C catalyst layer, this behavior was further studied via ICP-MS analysis. According to the protocol described in the experimental section the catalyst layer of Pt-C and Pt BR and AR was dissolved in aqua

regia to quantify the total catalyst loss. The latter of the two catalysts served as a comparison reference point for the detachment of the Pt-C. From the total catalyst loss and the dissolution amount the detachment degradation was quantified (Figure 10). The results, in Figure 12, indeed show a considerably higher detachment of Pt-C compared to Pt, accounting for more than 30% degradation of the total catalyst layer.

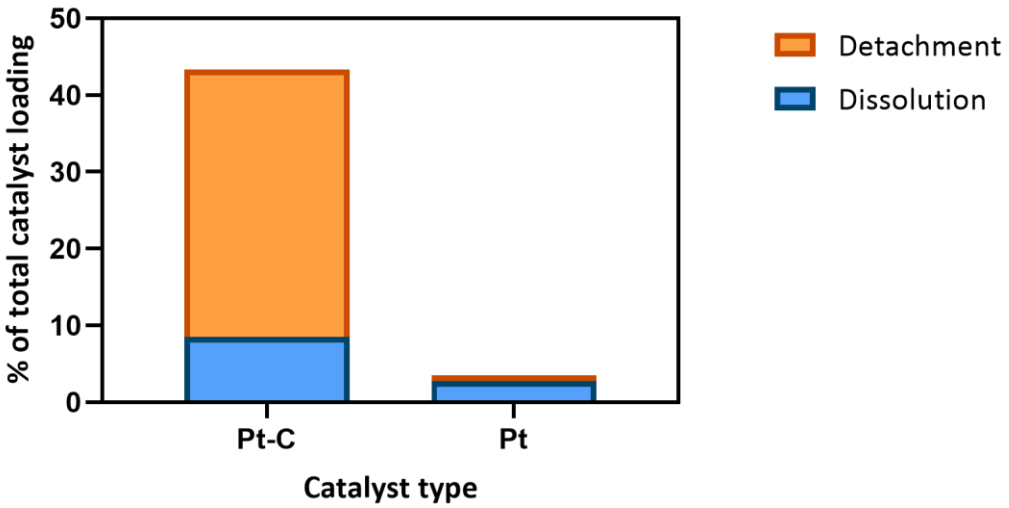

Figure 12: The detachment and dissolution degradation of Pt and Pt-C catalyst, quantified via ICP-MS analysis according to section 6 in materials and methods. The Pt and Pt-C samples underwent chronopotentiometric runs of 10 min each at 66.67, 88.89, 111.1, 133.3 and 155.6 mA/cm² at room temperature and 15 mL/min ethylene, 15 mL/min 0.5M KBr anolyte and 15 mL/min 0.5M KCl catholyte flow.

Figure 13 displays the optical microscopy image of a Pt (right) and Pt-C coating layer. As discussed the Pt-C material consists for only 20% out of Pt (and 80% carbon) as opposed to the 100% Pt content of the Pt black powder. Consequently the Pt-C coating contains five times more catalyst powder, and Nafion® binder, to maintain an equal catalyst loading of 1 mg/cm². Due to this higher solid content, the resulting coating is thicker, which covers the GDE more extensively as such blocking the gas pathways in the mesoporous layer. Given the flow-through operation of the reactor, the carbon supported catalyst layer is more susceptible to sustain

damage due to an increased pressure build up, i.e. detachment, when the ethylene feed passes through.

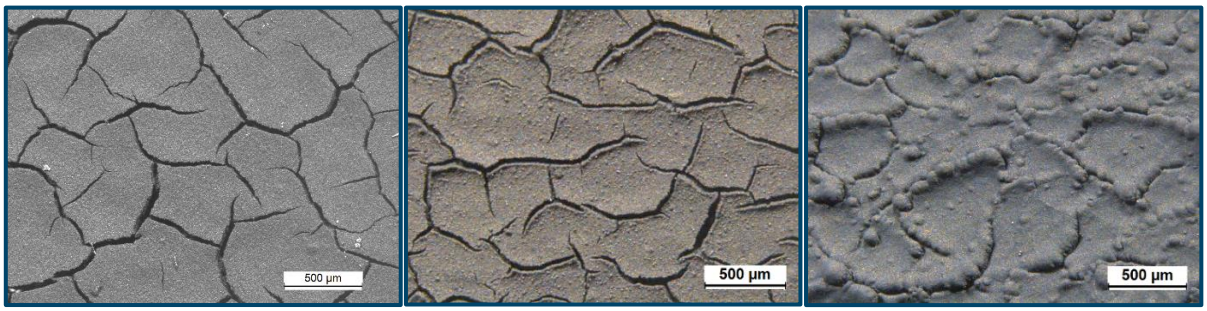

Figure 13: Optical microscopy images of an uncoated (left), Pt coated (middle) and Pt-C coated (right) mesoporous layer of the GDE substrate.

Conclusions

In this paper we demonstrated the high performance of the bromine mediated mechanism for EO production in a continuous flow-through reactor. Employing Pt, Pt-C and IrO_2 based GDE's the reactor maintained a high and stable FE towards EO between 80 to 90% for the tested current density range of 67 to 156 mA/cm², achieving in the best case an equivalent EO production of 1 kg/hour/m² in 0.5 M KBr anolyte. Furthermore GC analysis of the liquid and gas phase indicated the reactor setup to be fully selective towards the BER and the absence of OER and OOxR. The bromide inhibition effect on the OER, the low thermodynamical onset potential of the BER and the pH levels facilitated by the Nafion membrane (Figure 8) contribute to the fully selective BER and HER. Consequently the overall EO production is solely hampered by the formation of Br_2Et side product. As such, in order to elevate the EO selectivity even higher, the suppression of the Br_2Et formation is of outmost importance. To this end a backside gas channel in flow-through operation was implemented to achieve homogeneous dispersion of ethylene over the electrode surface to promote BrEtOH synthesis. The results indicate that an increased current density positively influences the disproportionation of bromine to hypobromous acid, which in turn promotes the synthesis of BrEtOH and suppresses Br_2Et.

For big scale electrochemical processes the power efficiency is a key parameter. In this regard the bromine mediated system holds an inherent advantage over the chlorine mediated system due to a considerably lower onset potential, i.e. 1.07V versus 1.36 V versus SHE. Overall the reactor system utilizing an IrO_2 coated anode proved to be the most potent in terms of selectivity, productivity and stability. Pt based materials are prone to dissolution degradation in the acidic oxidative conditions. Furthermore the Pt-C anode was susceptible to mechanically induced detachment, created by the exerted force of the ethylene feed in flow-through operation. Lastly the IrO_2-C configured reactor exhibited significantly lower EO selectivity and productivity figures.

Acknowledgements

Jonathan Schalck is supported by a Baekeland PhD grant (project no. HBC.2019.2163). Co-author Jonas Hereijgers is supported by the research foundation of Flanders (FWO) in the frame of a post-doctoral grant (project no. 1269021N & 1511819N). Furthermore the authors acknowledge the contribution of Lien Pacquets and Hannelore Andries for conducting the SEM, EDX and ICP-MS analyses in this work.

Sources

[1] J. M. Hollis, F. J. Lovas, P. R. Jewell, and L. H. Coudert, “INTERSTELLAR ANTIFREEZE: ETHYLENE GLYCOL,” 2002.

[2] S. Rebsdat and D. Mayer, “Ethylene Oxide,” *Ullmann’s Encycl. Ind. Chem.*, pp. 547–572, 2012.

[3] G. Floudas and C. Tssitisilianis, “Crystallization Kinetics of Poly(ethylene oxide) in Poly(ethylene oxide) - Polystyrene - Poly (ethylene oxide) Triblock Copolymers,” *Macromolecules*, vol. 9297, no. 96, pp. 4381–4387, 1997.

[4] T. Salmi, M. Roche, J. H. Carucci, K. Eränen, and D. Murzin, “Ethylene Oxide - kinetics and mechanism,” *Curr. Opin. Chem. Eng.*, vol. 1, no. 3, pp. 321–327, 2012.

[5] H. Lee, M. Ghanta, D. H. Busch, and B. Subramaniam, “Toward a CO 2 -free ethylene oxide process : Homogeneous ethylene oxide in gas-expanded liquids,” *Chem. Eng. Sci.*, vol. 65, no. 1, pp. 128–134, 2010.

[6] J. . Serafin, A. . Liu, and S. . Seyedmonir, “Surface science and the siver catalyzed

epoxidation of ethylene_an industrial perspective," *J. Mol. Catal. AC*, vol. 131, no. 1–3, pp. 157–168, 1998.

[7] International Energy Agency, International Council of Chemical Associations, and Dechema, "Technology Roadmap: Energy and GHG Reductions in the Chemical Industry via Catalytic Processes," 2013.

[8] C. Stegelmann, N. C. Schiødt, C. T. Campbell, and P. Stoltze, "Microkinetic modeling of ethylene oxidation over silver," *J. Catal.*, vol. 221, pp. 630–649, 2004.

[9] P. A. Kilty and W. M. H. Sachtler, "THE MECHANISM OF THE SELECTIVE OXIDATION OF ETHYLENE TO ETHYLENE," *Catal. Rev. Sci. Eng.*, vol. 10, no. September 2012, pp. 1–16, 1974.

[10] R. A. Van Santen and H. P. C. E. Kuipers, "The mechanism of ethylene epoxidation," *Adv. Catal.*, vol. 35, pp. 265–321, 1987.

[11] J. G. Vos and M. T. M. Koper, "Measurement of competition between oxygen evolution and chlorine evolution using rotating ring-disk electrode voltammetry," *J. Electroanal. Chem.*, vol. 819, no. July 2017, pp. 260–268, 2018.

[12] European Union, "EU ETS Handbook." European Union, p. 140, 2013.

[13] W. R. Leow *et al.*, "Chloride-mediated selective electrosynthesis of ethylene and propylene oxides at high current density," *Science (80-.).*, vol. 368, no. 6496, pp. 1228–1233, 2020.

[14] A. Winiwarter *et al.*, "Towards an atomistic understanding of electrocatalytic partial hydrocarbon oxidation: Propene on palladium," *Energy Environ. Sci.*, vol. 12, no. 3, pp. 1055–1067, 2019.

[15] M. C. Figueiredo, "Towards the sustainable synthesis of ethylene glycol," *Nat. Catal.*, no. 3, pp. 4–5, 2020.

[16] M. Chung, K. Jin, J. S. Zeng, and K. Manthiram, "Mechanism of Chlorine-Mediated Electrochemical Ethylene Oxidation in Saline Water," *ACS Catal.*, vol. 10, pp. 14015–14023, 2020.

[17] J. M. Bell and M. L. Buckley, "The solubility of bromin in aqueous solutions of sodium bromide," *J. Am. Chem. Soc.*, vol. 34, no. 1, pp. 15–15, 1912.

[18] B. Grinbaum and M. Freiberg, *Kirk-Othmer Encyclopedia of Chemical Technology*. Wiley, 2000.

[19] J. Ghoroghchian, R. E. W. Jansson, and D. Jones, "The production of hypobromite and of propylene oxide in an electrochemical pump cell," *J. Appl. Electrochem.*, pp. 437–443, 1977.

[20] A. Manji and C. W. Oloman, "Electrosynthesis of propylene oxide in a bipolar trickle-bed reactor," *J. Appl. Electrochem.*, vol. 17, no. 3, pp. 532–544, 1987.

[21] V. Yarlagadda, R. P. Dowd, J. W. Park, P. N. Pintauro, and T. Van Nguyen, "A comprehensive study of an Acid Based Reversible H2Br2 Fuel cell system," *J. Electrochem. Soc.*, vol. 162, p. F919, 2015.

[22] T. Truc, T. L. Yu, and H. Lin, "Influence of the composition of isopropyl alcohol / water mixture solvents in catalyst ink solutions on proton exchange membrane fuel cell

performance," *J. Power Sources*, vol. 225, pp. 293–303, 2013.

[23] M. Goor-Dar, N. Travitsky, and E. Peled, "Study of OER and HER on Pt nanoparticles in concentrated HBr solutions," *J. Power Sources*, vol. 197, pp. 111–115, 2012.

[24] V. Livshits, A. Ulus, and E. Peled, "High-power H 2 / Br 2 fuel cell," *Electrochem. commun.*, vol. 8, pp. 1358–1362, 2006.

[25] S. Geiger *et al.*, "The stability number as a metric for electrocatalyst benchmarking," *Nat. Catal.*, pp. 508–515, 2018.

[26] M. Verniette, C. Daremon, and J. Simonet, "DE LIAISONS INSATUREES NUCLEOPHILES - COMPORTEMENT DES DERIVES ETHYLENIQUES ET ACETYLENIQUES," *Electrochim. Acta*, 1977.

[27] K. A. V'yunov and A. I. Ginak, "Related content The Mechanism of the Electrophilic Addition of Halogens to a Multiple Bond," *Russ. Chem. Rev.*, vol. 2, pp. 273–295, 1981.

[28] J. A. M. Leduc, "Electrochemical process for the production of organic oxides," US3288692A, 1962.

[29] B. E. Conway, Y. Phillips, and S. Y. Qian, "Surface Electrochemistry and Kinetics of anodic Bromine Formation at Platinum," *J. Chem. Soc. Faraday Trans.*, vol. 91, no. 2, pp. 293–293, 1995.

[30] G. Afonso, B. Mello, V. Briega-martos, V. Climent, and J. M. Feliu, "Bromide Adsorption on Pt (111) Over a Wide Range of pH : Cyclic Voltammetry and CO Displacement Experiments," *J. Phys. Chem. C*, vol. 122, no. 32, pp. 18562–18569, 2018.

[31] H. A. Gasteiger, N. M. Markovic, and P. N. Ross, "Bromide Adsorption on Pt (111): Adsorption Isotherm and Electrosorption Valency Deduced from RRD Pt (111) E Measurements," *Langmuir*, no. 111, pp. 1414–1418, 1996.

[32] W. A. Braff, M. Z. Bazant, and C. R. Buie, "Membrane-less hydrogen bromine flow battery," *Nat. Commun.*, 2013.

[33] V. Krstic and B. Pesoviski, "Reviews the research on some dimensionally stable anodes (DSA) based on titanium.," *Hydrometallurgy*, vol. 185, pp. 71–75, 2019.